

# Command of Collective Dynamics by Topological Defects in Spherical Crystals

Zhenwei Yao\*

*School of Physics and Astronomy, and Institute of Natural Sciences,  
Shanghai Jiao Tong University, Shanghai 200240, China*

Directing individual motions of many constituents to coherent dynamical state is a fundamental challenge in multiple fields. Here, based on the spherical crystal model, we show that topological defects in particle arrays can be a crucial element in regulating collective dynamics. Specifically, we highlight the defect-driven synchronized breathing modes around disclinations and collective oscillations with strong connection to disruption of crystalline order. This work opens the promising possibility of an organizational principle based on topological defects, and may inspire new strategies for harnessing intriguing collective dynamics in extensive nonequilibrium systems.

Understanding self-organization of individual motions of many constituents into coherent motions is a fundamental and practical problem in multiple fields ranging from many-body problems [1, 2], active matter [3–6] to biological processes [7, 8]. Highly ordered collective motions in far-from-equilibrium many-body systems can be driven by active processes [4, 5], physical interactions [9–11], and exchange of signals [7, 12, 13]. Recently, carefully designed lattice structures have been used to guide collective motions of particles [14], and host exotic unidirectional sound modes [15, 16]. These studies suggest an organizational principle based on establishing lattice structure among constituents. While the connection of particle density and collective motion has been extensively studied in various active matter systems [17–20], the question of how the crystallographic structures in particle arrays, particularly the defects therein, regulate the collective dynamics has not yet been fully explored. Since collective motions can be characterized by singularities in the velocity vector field [20], elucidating the interplay of the defects in particle arrays and the vector field may inspire new strategies for harnessing intriguing collective dynamics in extensive nonequilibrium systems.

The spherical crystal model provides a suitable tool to address these questions. A spherical crystal refers to a two-dimensional crystal lattice wrapping the entire sphere. Crystallographic defects, known as topological defects, are inevitable in the spherical crystal as demanded by topological constraints [21–23]. Repulsive point particles on the sphere spontaneously form a crystal. Determining its ground state is a 100-year-old puzzle known as the Thomson problem [24], which has strong connections with virus morphology [25, 26] and various geometric frustrations of condensed matters [22, 27–31]. In our model, we introduce dynamics by imposing random disturbance to the lowest-energy spherical crystal composed of long-range repulsive particles. By numerically integrating the equations of motion at high precision, we reveal highly symmetric singularity structures in the velocity vector field. The crucial element for shaping

such a well-organized velocity field is the synchronized breathing modes around the twelve disclinations. We further identify a collective oscillation mode that is closely related with disruption of crystalline order. These two kinds of collective dynamical modes are generic in spherical crystals of distinct symmetries at varying strength of disturbance. These results demonstrate how dynamical order can be achieved by topological defects in particle arrays, and may have implications in commanding the nonequilibrium dynamics of active matters.

In our model, we consider a collection of point particles confined on the sphere interacting by the Coulomb potential  $V(r) = \beta/r$ , where  $r$  is the Euclidean distance between two particles, and  $\beta$  is a constant. According to the Euler's theorem, topological defects are inevitable in the spherical crystal [23]. The elementary topological defects in two-dimensional triangular lattices are  $n$ -fold disclinations, which are vertices whose coordination number  $n$  is deviated from 6. Euler's theorem states that on a closed triangulated surface  $M$ ,

$$\sum_i q_i = 2\pi\chi(M), \quad (1)$$

where  $q_i$  is the topological charge of the vertex  $i$ , and  $\chi(M)$  is Euler's characteristic [23].  $q_i = (6 - n)\pi/3$  for a vertex with coordination number  $n$ .  $\chi(M) = 2$  for the sphere, so topological defects are inevitable in the spherical crystal. Following the Caspar-Klug scheme, we construct the basic structure of the spherical crystal whose twelve fivefold disclinations are located at the vertices of an inscribed icosahedron [25]. All possible crystal lattices in the Caspar-Klug construction are represented by a pair of non-negative integers  $(p, q)$ . The  $q$  value reflects distinct symmetries of the spherical crystal.

We introduce dynamics by imposing random disturbance to the lowest-energy configuration of the spherical crystal obtained by the steepest descent method [32, 33]. Specifically, we pull each particle away from its balance position by a displacement  $\delta\vec{x}$ .  $\delta\vec{x} = \Gamma a(\cos\alpha, \sin\alpha)$  in the unit basis vectors  $\{\hat{e}_\theta, \hat{e}_\phi\}$ .  $a$  is the lattice spacing.  $\Gamma a$  and  $\alpha$  are the magnitude and direction of the particle displacement.  $\alpha$  is a uniform random variable in  $[0, 2\pi)$ . The ensuing evolution of the system is governed by the

---

\*Electronic address: zyao@sjtu.edu.cn

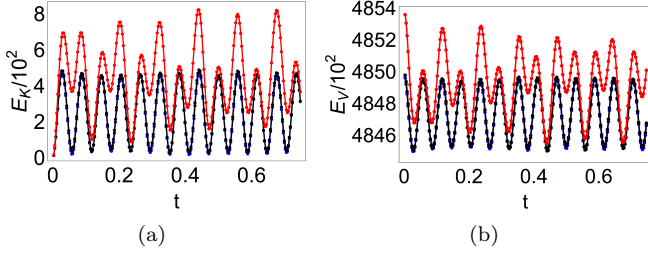


FIG. 1: Evolution of total kinetic and potential energies of disturbed spherical crystals. The total energy is well conserved. The amplitude of disturbance  $\Gamma = 1\%$  (blue),  $10\%$  (black), and  $40\%$  (red).  $(p, q) = (10, 0)$ .

following equations of motion in spherical coordinates:

$$\begin{aligned} mR^2\ddot{\theta}_i &= mR^2\dot{\phi}_i^2 \sin\theta_i \cos\theta_i - \sum_{j \neq i} \frac{\partial V(r_{ij})}{\partial \theta_i}, \\ mR^2 \frac{d}{dt} (\sin^2 \theta_i \dot{\phi}_i) &= - \sum_{j \neq i} \frac{\partial V(r_{ij})}{\partial \phi_i}. \end{aligned} \quad (2)$$

We numerically integrate Eqs.(2) for the particle trajectories with various given initial conditions at high precision (see Supplemental Material for technical details). The approach based on the equations of motion allows us to explore the regime of large disturbance that is beyond the scope of perturbation analysis. The length, mass and time are measured in the units of the spherical radius  $R$ , particle mass  $m$ , and  $\tau_0 = R\sqrt{m/\epsilon_0}$ , where  $\epsilon_0 = \beta/R$ .

We first track the temporally varying total kinetic and potential energies, as shown in Fig. 1. In the spherical system, the relation between the kinetic and potential energies does not conform to the Virial theorem because of the extra contribution from the constraint of the sphere to the force on a particle [34]. From Fig. 1, we see that for small  $\Gamma$ , where the initial displacements of the particles from their balance positions are small in comparison with the lattice spacing, the energy curves are sinusoidal. With the increase of  $\Gamma$ , the energy curves exhibit double-peak structures as shown in the red curves for  $\Gamma = 40\%$ . Note that in even longer simulation time (up to 1.5 million simulation steps;  $t = 1.5$ ) the energy curves still exhibit oscillating behaviors featured with the double-peak structure, and the crystalline order of the system is well preserved. The periodic oscillation of the energy curves suggests ordered dynamical modes underlying the particle motions.

Prior to examining the dynamical modes on the sphere, we first present general discussions about the topology of a vector field on the sphere. As a classical problem of differential topology, an even-dimensional sphere admits no regular tangent vector field, and singularities are inevitable as a topological constraint [35]. A singularity at point  $p$  in the vector field  $V$  is characterized by its index

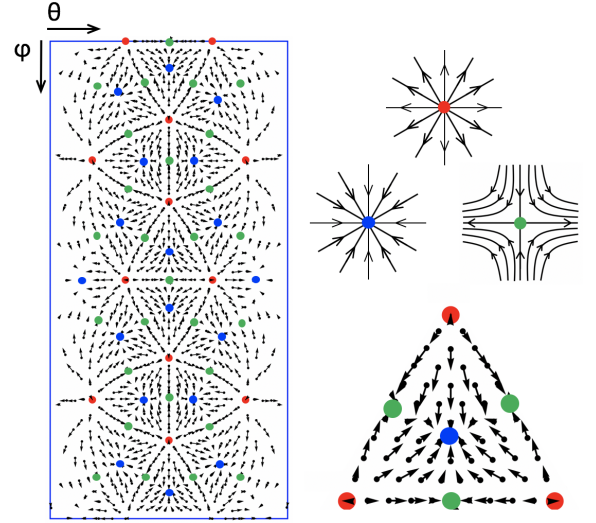


FIG. 2: Highly symmetric velocity vector field regulated by the twelve disclinations (indicated by red dots) in the spherical crystal. The particle configuration is represented in the spherical coordinates  $(\theta, \phi)$ . The entire velocity field is equally compartmented into identical subfields in the spherical triangles spanned by three neighboring disclinations; a zoomed-in plot of a subfield is shown in the lower right panel. The three types of singularities are also schematically shown.  $\Gamma = 1\%$ .  $t = 0.735$ .  $(p, q) = (10, 0)$ .

$\text{Ind}_p V$ :

$$\text{Ind}_p V = \frac{1}{2\pi} \oint_{\gamma} d\theta, \quad (3)$$

where  $\theta$  specifies the direction of the vector field along a closed contour  $\gamma$ .  $\text{Ind}_p V \in \mathbb{Z}$ . Remarkably, there is a deep connection between vector fields and topology illustrated by the Poincaré-Hopf index theorem [36]. It states that, over a compact manifold  $M$  without boundary, regardless of the chosen vector field  $V$ ,

$$\sum_{p \in M} \text{Ind}_p V = \chi(M). \quad (4)$$

Applying Eq.(4) on the 2-sphere, we obtain the hairy ball theorem:  $\sum_{p \in \mathbb{S}^2} \text{Ind}_p V = 2$ . The name of this theorem is related to the fact that it is impossible to comb the hairs without creating a cowlick. Equation (4) dictates a topological constraint on the configuration of the vector field on the sphere. It is natural to ask how the defects in the spherical crystal will shape the velocity field and regulate the topologically required singularities therein.

In Fig. 2, we present a typical snapshot of the instantaneous velocity vector field. The red dots are the preexistent fivefold disclinations in the spherical crystal; they are located at the vertices of an inscribed icosahedron. Remarkably, the entire velocity field is equally compartmented into identical subfields in the spherical triangles spanned by three neighboring disclinations. We identify three types of singularities in the velocity field: sources

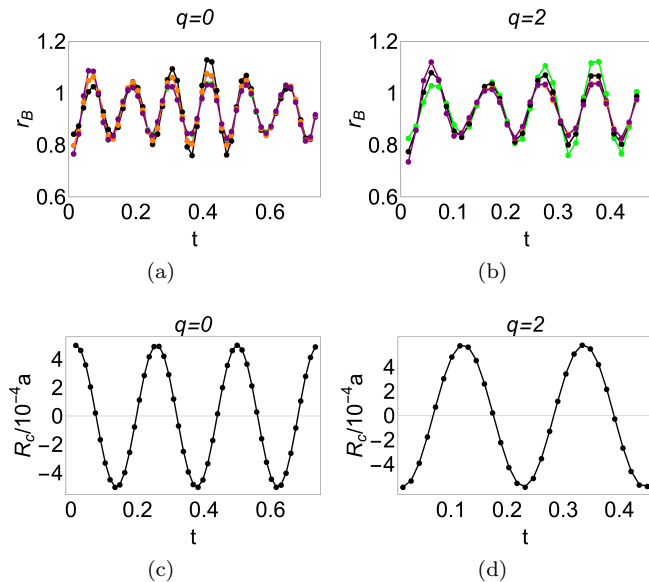


FIG. 3: Two kinds of dynamical modes revealed in the collective dynamics of the spherical crystals with distinct symmetries. (a) and (b) show the synchronization of the breathing modes around the twelve disclinations.  $r_B$  is the average distance from the disclination to the five neighboring particles. (c) and (d) show the collective oscillation mode.  $R_c$  is the location of the center of mass on the  $z$  axis. The amplitude of oscillation is only at the order of ten-thousandth of the lattice spacing  $a$ .  $\Gamma = 1\%$ .  $p = 10$ .

(red dots), sinks (blue dots), and saddle points (green dots), whose indices are  $+1$ ,  $+1$ , and  $-1$ , respectively. The entire velocity field is characterized by the highly symmetric arrangement of these singularities. Specifically, the 20 blue dots and 30 green dots are located at the vertices of the inscribed dodecahedron and icosidodecahedron, respectively. We also present the evolution of the velocity field and the slight displacement of the singularity structure in Supplemental Material. We count the total index value to be exactly  $+2$ . Notably, the vector field configuration in Fig. 2 has been used to prove the hairy ball theorem [35]. For spherical crystals with nonzero  $q$ , the velocity fields exhibit identical defect structure as in Fig. 2; the typical velocity fields for  $q = 2, 3$ , and  $6$  are presented in Supplemental Material. It indicates that the highly symmetric singularity structure is a generic feature in the velocity field of the spherical crystals.

Spatiotemporal analysis of the velocity field reveals alternating inward and outward movement of the five neighboring particles surrounding each disclination. Such a breathing mode is crucial for fabricating the highly symmetric velocity field. We quantitatively characterize the breathing mode by introducing the quantity  $r_B(t)$ , which is the temporally varying average distance from the disclination to the five neighboring particles. The coincidence of the  $r_B - t$  curves of the twelve discli-

nations in Fig. 3(a) indicates the spontaneous synchronization of the local breathing modes. And the transition to this ordered dynamical state is a fast process (in comparison with the breathing period). This salient feature is also found in spherical crystals with distinct symmetries; a typical case of  $q = 2$  is shown in Fig. 3(b).

We further inquire under which conditions the breathing mode will emerge. We examine spherical crystals of all kinds of symmetries for  $q \in [0, p]$ , and vary the value of  $\Gamma$  from 0.1% up to 25%. It turns out that both the frequency and amplitude (measured by the lattice spacing) of the breathing mode are independent of the  $\Gamma$  and  $q$  values. It is noteworthy that changing the  $q$  value leads to the variation of the number of particles. So the emergence of the breathing mode is also independent of particle density, which is due to the lack of a length scale in the potential  $V(r)$ . Furthermore, we disturb the system in various ways, such as using a series of random initial states with randomly distributed  $\Gamma$ , disturbing randomly picked particles, disturbing only the disclinations, etc. In all these cases, the system quickly enters the dynamical state of synchronized breathing modes.

To explore the origin of the breathing mode, we perform normal mode analysis for the elementary pentagonal configuration, and find that the radial eigenmode is exactly the mode selected by the system to fabricate the breathing mode (see Supplemental Material). Furthermore, from the perspective of symmetry, such a mode preserves the local fivefold rotational symmetry around the disclination. As a numerical observation to substantiate this viewpoint, we find that once an isolated fivefold disclination is converted to a scar that is composed of alternating five and sevenfold disclinations, i.e., the local fivefold symmetry is broken, the breathing mode also vanishes [22]. Note that in this disclination-scar conversion, the bond-orientational order is still preserved [23]. From the perspective of energetics, the symmetry-broken dynamical mode around the disclinations seems unfavored. We design a symmetry-broken dynamical mode by moving a disclination and a randomly picked undefected particle towards their neighboring particles respectively. In this process, the system energy of the former case increases much faster, indicating that a symmetry-broken dynamical mode around the disclination is energetically unfavored.

The double-peak structure in the red energy curves in Fig. 1 implies a new dynamical mode supported in the spherical crystal system. To identify this mode, extensive data analysis of the numerical results leads us to examine the trajectory of the center of mass of the system. It turns out that the center-of-mass trajectory coincides with the two-fold axis of the icosahedron spanned by the twelve disclinations that passes through the midpoints of the two opposite edges. By setting this line to be the  $z$  axis, we reveal a small-amplitude collective oscillation of the system along the  $z$  axis, as shown in Fig. 3(c) and 3(d). This dynamical mode is pervasive in spherical crystals with distinct symmetries, with scars (which

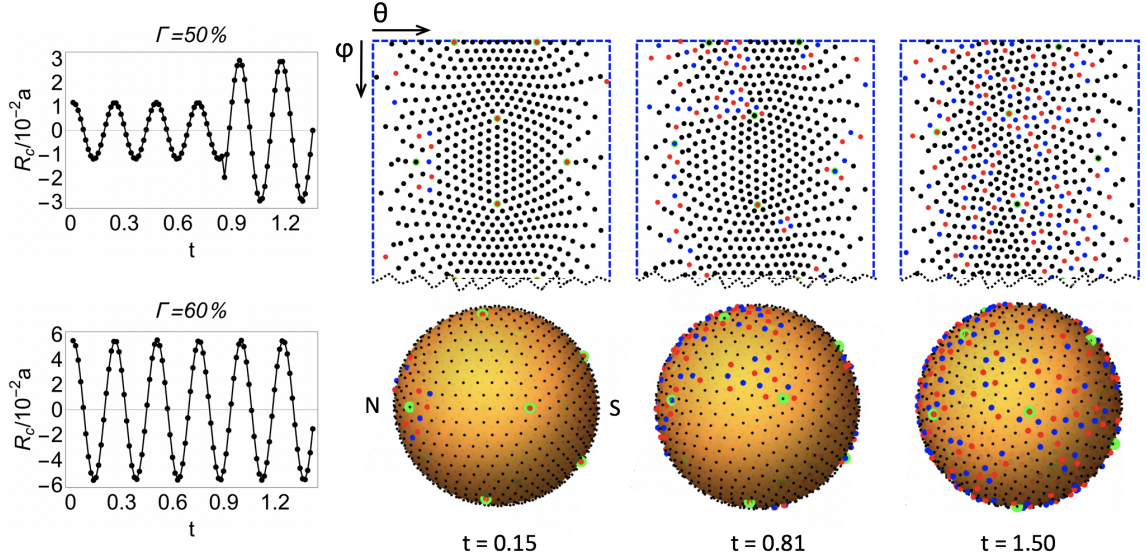


FIG. 4:  $\Gamma$ -driven disruption of crystalline order in the spherical crystal. Left panels show the collective oscillation at  $\Gamma = 50\%$  and  $\Gamma = 60\%$ .  $R_c$  is the location of the center of mass on the  $z$  axis. The three snapshots of particle configurations at  $\Gamma = 60\%$  plotted in the spherical coordinates and on the sphere show the migration of the emergent defects (colored dots) from the poles of the sphere to the equatorial region during a few collective oscillations. Green dots represent the pre-existent twelve disclinations. Red and blue dots are five- and seven-fold disclinations.  $(p, q) = (10, 0)$ .

are line defects out of isolated point disclinations), and even with disrupted crystalline order. In contrast, the breathing mode is suppressed in the latter two cases. The ubiquity and the small-amplitude features of the collective oscillation mode imply that this is a fundamental dynamical mode in the spherical crystal system. A systematic survey in the parameter space of  $q$  and  $\Gamma$  (prior to disruption of crystalline order) shows that the ratio of the frequencies of the temporally varying kinetic energy, the breathing mode and the collective oscillation mode is a constant:

$$w_E : w_B : w_O = 1 : \frac{1}{2} : \frac{1}{4}. \quad (5)$$

In comparison with Fig. 1, we identify the collective oscillation as the dynamical mode underlying the double-peak structure in the energy curves.

We proceed to discuss the connection of the collective oscillation mode and the disruption of the spherical crystal. The failure of the particles to be restored at sufficiently large disturbance is the microscopic origin of the  $\Gamma$ -driven disruption of crystalline order. As a signal of phase transition, we find the abrupt increase of the amplitude of the collective oscillation, as shown in the left upper panel in Fig. 4 when  $\Gamma = 50\%$ . The system is softened in the sense of the significantly enhanced oscillation amplitude. What is the origin of the softening effect? Frame-by-frame analysis of the Delaunay-triangulated particle configurations shows that the softening of the system occurs exactly upon the appearance of topological defects [23]. In a static system, the appearance of crystalline defects tends to reduce stress [23, 39]. Here, through the softening phenomenon, we show the

dynamic effect of topological defects.

From the characteristic snapshots in the disruption process of crystalline order at larger  $\Gamma$  as shown in Fig. 4, we see the migration of the emergent defects (indicated by colored dots) from the poles of the sphere to the equatorial region during a few collective oscillations. The connection of the collective oscillation mode and the characteristic events in the disruption process, such as the softening of the system and the global migration of defects, may be attributed to its long-wavelength nature; long-wavelength fluctuations make dominant contribution in phase transition [23]. The snapshots in Fig. 4 also show that in the disruption process the relative positions of the preexistent disclinations (in green dots) are subject to large deviation due to the softening of the crystal lattice (see Supplemental Material for quantitative analysis of the drift process of the disclinations).

In summary, by combination of numerical simulations and analytical normal mode analysis, we have shown that topological defects in particle arrays can be a crucial element in regulating collective dynamics and achieving dynamic order. Specifically, we highlight two generic dynamical modes: synchronized breathing modes around disclinations that induce highly symmetric singularity structures in the velocity vector field, and collective oscillation with strong connection to disruption of crystalline order. These results suggest an organizational principle based on crystalline defects, and may inspire new strategies for harnessing intriguing collective dynamics in extensive nonequilibrium systems.

This work was supported by NSFC Grants No. 16Z103010253, the SJTU startup fund under Grant No.

WF220441904, and the award of the Chinese Thousand Talents Program for Distinguished Young Scholars under

Grant No. 17Z127060032, and No.18Z127060018.

- 
- [1] F. Calogero, *Classical Many-Body Problems Amenable To Exact Treatments* (Springer Science & Business Media, 2003).
  - [2] H. Bruus and K. Flensberg, *Many-Body Quantum Theory in Condensed Matter Physics* (Oxford University Press, 2004).
  - [3] T. Vicsek, A. Czirók, E. Ben-Jacob, I. Cohen, and O. Shochet, Phys. Rev. Lett. **75**, 1226 (1995).
  - [4] M.C. Marchetti, J.F. Joanny, S. Ramaswamy, T.B. Liverpool, J. Prost, M. Rao, and R. A. Simha, Rev. Mod. Phys. **85**, 1143 (2013).
  - [5] F. C. Keber, E. Loiseau, T. Sanchez, S. J. DeCamp, L. Gioni, M. J. Bowick, M. C. Marchetti, Z. Dogic, and A. R. Bausch, Science **345**, 1135 (2014).
  - [6] N. H. P. Nguyen, D. Klotz, M. Engel, and S. C. Glotzer, Phys. Rev. Lett. **112**, 075701 (2014).
  - [7] D. Bray, *Cell Movements: From Molecules to Motility* (Garland Science, 2000).
  - [8] S. Wang and P. G. Wolynes, Proc. Natl. Acad. Sci. U.S.A. **108**, 15184 (2011).
  - [9] S. Chattopadhyay and X.-L. Wu, Biophys. J. **96**, 2023 (2009).
  - [10] M. Nitzan, J. Casadiego, and M. Timme, Sci. Adv. **3**, e1600396 (2017).
  - [11] P. Mandal, G. Patil, H. Kakoty, and A. Ghosh, Acc. Chem. Res. **51**, 2689 (2018).
  - [12] D. Helbing, I. Farkas, and T. Vicsek, Nature **407**, 487 (2000).
  - [13] C. Chen, S. Liu, X.-q. Shi, H. Chaté, and Y. Wu, Nature **542**, 210 (2017).
  - [14] Z. Yao, Phys. Rev. E **96**, 062139 (2017).
  - [15] Z. Yang, F. Gao, X. Shi, X. Lin, Z. Gao, Y. Chong, and B. Zhang, Phys. Rev. Lett. **114**, 114301 (2015).
  - [16] S. Shankar, M. J. Bowick, and M. C. Marchetti, Phys. Rev. X **7**, 031039 (2017).
  - [17] H.-P. Zhang, A. Beer, E.-L. Florin, and H. L. Swinney, Proc. Natl. Acad. Sci. U.S.A. **107**, 13626 (2010).
  - [18] T. Vicsek and A. Zafeiris, Phys. Rep. **517**, 71 (2012).
  - [19] Y. Sumino, K. H. Nagai, Y. Shitaka, D. Tanaka, K. Yoshikawa, H. Chaté, and K. Oiw, Nature **483**, 448 (2012).
  - [20] V. Schaller and A. R. Bausch, Proc. Natl. Acad. Sci. U.S.A. **110**, 4488 (2013).
  - [21] M. Bowick, A. Cacciuto, D. R. Nelson, and A. Travesset, Phys. Rev. Lett. **89**, 185502 (2002).
  - [22] A. Bausch, M. Bowick, A. Cacciuto, A. Dinsmore, M. Hsu, D. Nelson, M. Nikolaides, A. Travesset, and D. Weitz, Science **299**, 1716 (2003).
  - [23] D. R. Nelson, *Defects and Geometry in Condensed Matter Physics* (Cambridge University Press, Cambridge, 2002).
  - [24] J. J. Thomson, Philos. Mag. **7**, 237 (1904).
  - [25] D. L. Caspar and A. Klug, in *Cold Spring Harbor Symposium on Quantitative Biology* (Cold Spring Harbor Laboratory Press, 1962), vol. 27, pp. 1–24.
  - [26] J. Lidmar, L. Mirny, and D. R. Nelson, Phys. Rev. E **68**, 051910 (2003).
  - [27] A. Dinsmore, M. F. Hsu, M. Nikolaides, M. Marquez, A. Bausch, and D. Weitz, Science **298**, 1006 (2002).
  - [28] Z. Yao, Soft Matter **13**, 5905 (2017).
  - [29] W. T. Irvine, V. Vitelli, and P. M. Chaikin, Nature **468**, 947 (2010).
  - [30] A. Azadi and G. M. Grason, Phys. Rev. Lett. **112**, 225502 (2014).
  - [31] D. Mehta, J. Chen, D. Chen, H. Kusumaatmaja and D. J. Wales, Phys. Rev. Lett. **117**, 028301 (2016).
  - [32] Z. Yao and M. Olvera de la Cruz, Phys. Rev. Lett. **111**, 115503 (2013).
  - [33] Z. Yao and M. Olvera de la Cruz, Phys. Rev. Lett. **116**, 148101 (2016).
  - [34] H. Goldstein, *Classical Mechanics* (Addison-Wesley Pub. Co., 1980).
  - [35] Y. Aminov, *Geometry of Vector Fields* (CRC Press, 2000).
  - [36] P. Renteln, *Manifolds, Tensors, and Forms: An Introduction for Mathematicians and Physicists* (Cambridge University Press, 2013).
  - [37] J. C. Maxwell, Philos. Mag. **27**, 294 (1864).
  - [38] V. Vitelli, Proc. Natl. Acad. Sci. U.S.A. **109**, 12266 (2012).
  - [39] B. Audoly and Y. Pomeau, *Elasticity and Geometry* (Oxford Univ. Press, 2010).